DRUG DELIVERY
2022, VOL. 29, NO. 1, 1232–1242
https://doi.org/10.1080/10717544.2022.2053761

Taylor & Francis
Taylor & Francis Group

RESEARCH ARTICLE

OPEN ACCESS Check for updates

# Hyaluronan-modified transfersomes based hydrogel for enhanced transdermal delivery of indomethacin

Ming Yuan*, Jiangxiu Niu*, Qinghan Xiao, Huiyuan Ya, Yansong Zhang, Yanli Fan, Lingmei Li and Xueke Li

College of Food and Drug, Henan Functional Cosmetics Engineering & Technology Research Center, Luoyang Normal University, Luoyang, People's Republic of China

**ABSTRACT**

Hyaluronic acid (HA), as a hygroscopic and biocompatible molecule, has displayed unique permeation enhancement in transdermal delivery systems. Hence, indomethacin (IND) was encapsulated in HA-modified transfersomes (IND-HTs) to enhance transdermal IND delivery to reduce adverse effects in this study. The physiochemical properties of IND-HTs were characterized. Results showed that the prepared IND-HTs were spherical and revealed good entrapment efficiency (87.88 ± 2.03%), with a nanometric particle size (221.8 ± 93.34 nm). Then, IND-HTs were further incorporated into a carbopol 940 hydrogel (IND-HTs/Gel) to prolong retention capacity on the skin. The *in vitro* release and skin permeation experiments of IND-HTs/Gel were carried out with the Franz diffusion cells. It was found that IND-HTs/Gel exhibited sustained drug release, as well as superior drug permeation and flux across the skin. Confocal laser scanning microscopy showed improved penetration of HTs/Gel with a wider distribution and higher fluorescence intensity. The hematoxylin–eosin stained showed that HA improved the transdermal effect by changing the microstructure of skin layers and decreasing skin barrier function. In addition, IND-HTs/Gel showed significant analgesic activity in hot plate test and no potentially hazardous skin irritation. This study indicated that the developed IND-HTs/Gel could be a promising alternative to conventional oral delivery of IND by topical administration.

**ARTICLE HISTORY**
Received 21 January 2022
Revised 4 March 2022
Accepted 7 March 2022

**KEYWORDS**
Transdermal drug delivery; transfersome; hydrogel; indomethacin; hyaluronan

## Introduction

Transdermal drug delivery system (TDDS) is a route of topical administration delivered drugs through the skin, which exhibits many advantages such as bypass of first-pass effect, improved patient compliance, avoidance of gastrointestinal side effect, ease of self-administration, a more uniform peak plasma level of drug, and suitable long-term treatment (Alkilani et al., 2015; Sala et al., 2018). However, delivery of drugs across the skin barrier is highly challenging. Stratum corneum (SC), the outermost layer of the epidermis, serves as a major barrier for the skin. The presence of 10–15 layers of thick corneocytes, lipid matrix, corneodesmosomes, and tight junctions makes SC compact and impermeable to drug molecules (Andrews et al., 2013; Qindeel et al., 2020).

During these last decades, many attempts have been made to enhance drug permeation across the skin/SC barrier, including nanoparticle-based drug delivery system, such as liposomes. Conventional liposomes, typically composed of phospholipids and cholesterol, have been widely investigated as drug carriers for dermal route (Mura et al., 2007). However, the penetration of conventional liposomes is apparently confined to the SC and upper skin layers acting as a local drug reservoir with minimal penetration to deeper skin layers (Touitou et al., 2000).

Therefore, novel lipid vesicles have been proposed to improve the penetration ability of liposomes by increasing bilayer fluidity. Transfersomes, superior over conventional liposomes, are composed of several phospholipid bilayers with an addition component, i.e. the edge activator (EA). The added EA can be inserted between the phospholipids, disrupting the organization of the bilayer and making the transfersomes elastic and flexible (Ascenso et al., 2015; Sala et al., 2018; Salim et al., 2020). Transfersomes can easily deform and penetrate in an intact form into the deeper layers of the skin by being squeezed through the intercellular spaces of the SC, thus localizing the incorporated drug at high concentrations (Maestrelli et al., 2010; Abd El-Alim et al., 2019; Rabia et al., 2020). Moreover, EA can act as a permeation enhancer, disrupting the highly organized intercellular lipids from the SC and therefore facilitating the drug permeation (Singh et al., 2015).

Hyaluronic acid (HA), a natural linear glycosaminoglycan, is a major component of the extracellular matrix and is present in the skin at high concentrations (Laurent & Fraser, 1992). Recently, HA has been widely used in transdermal formulations to enhance the delivery efficacy. It is reported that

**CONTACT** Jiangxiu Niu niujxiu1982@126.com; Huiyuan Ya yahuiyuan@lynu.edu.cn College of Food and Drug, Henan Functional Cosmetics Engineering & Technology Research Center, Luoyang Normal University, Luoyang, Henan 471934, People's Republic of China
*Both authors contributed equally to this work.

low molecular weight HA (5–50 kDa) displays higher permeation enhancement effect as compared with medium (100–300 kDa) and high (600–1200 kDa) molecular weight ones (Zhu et al., 2020). Various mechanisms of HA mediated skin penetration are discussed involving skin hydration, HA receptor mediated transport, hydrophobic interaction with the SC and viscoelastic property. Due to its excellent hygroscopic property, HA is able to hydrate both the SC and the dermis. The extensive hydration will lead to swollen corneocytes, creating intercorneocyte ruptures, changing the microstructural of intercellular lipids, and eventually facilitating the permeation through the hydrated skin (Son et al., 2017). In addition, the hydrophobic domain of HA can interact with SC and decrease skin barrier function. The viscoelastic property of HA could retain the drugs in epidermis for a longer time (Yang et al., 2012).

Indomethacin (IND), a non-steroidal anti-inflammatory drug (NSAID), is widely used in treatment of chronic pain and inflammatory conditions such as rheumatoid arthritis, spondylosis deformans, and acute gout syndrome (Guermech et al., 2019). However, the oral administration of IND is usually accompanied by a number of adverse effects, including dyspepsia, peptic ulceration, and gastrointestinal disturbances. The adverse effects of IND can be divided into two categories, i.e. (i) topical irritancy and (ii) suppression of prostaglandin synthase activity (El-Leithy et al., 2015). In cases of chronic inflammatory diseases, patient noncompliance represents a prevailing therapeutic problem owing to long treatment periods in addition to the multiple daily doses required to ensure therapeutic blood levels (Abd El-Alim et al., 2019). Thus, the transdermal delivery of IND represents a promising alternative aiming to avoid the drawbacks associated with the oral route, which is more suitable for long-term treatment of chronic diseases.

In the present study, we constructed HA-modified transfersomes (IND-HTs; Figure 1) as an efficient nanovesicular carrier of IND for improved percutaneous permeation. To increase the skin retention property of IND-HTs, carbopol 940 hydrogel was employed as a reservoir to entrap the IND-HTs (Batool et al., 2021; Khan et al., 2022). The IND-HTs-embedded hydrogel (IND-HTs/Gel) could be painted as a patch on the skin with prolonged retention time in comparison with the IND-HTs solution. The IND-HTs were able to efficiently penetrate through skins by virtue of a combination of the disruption on skin barriers by HA and the favorable deformability of transfersomes, thus localizing IND at high concentration. The physicochemical properties of IND-HTs, *in vitro* skin permeation and *in vivo* treatment of IND-HTs/Gel were investigated.

## Materials and methods

### Materials

HA (MW <10 kDa) was obtained from Freda Biochem Co., Ltd. (Jinan, China). Octadecylamine (ODA) and IND were purchased from Aladdin (Shanghai, China). Soybean phospholipids (SPCs) were purchased from BASF (Ludwigshafen, Germany). Sodium deoxycholate was purchased from Shanghai EKEAR Biotechnology Co., Ltd. (Shanghai, China). 1-(3-Dimethylaminopropyl)-3-ethylcarbodiimide hydrochloride (EDC·HCl) and N-hydroxysuccinimide (NHS) were purchased from Nanjing Dulai Biotechnology Co., Ltd. (Nanjing, China). Coumarin-6 (Cou6) was purchased from Hefei Bomei

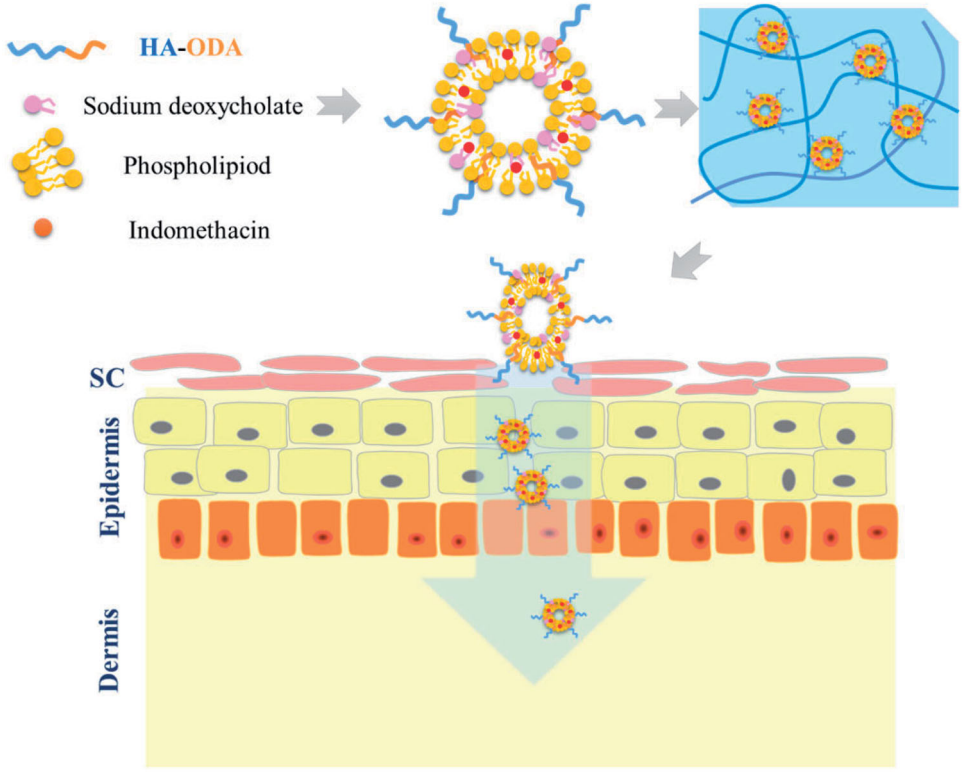


**Figure 1.** Schematic illustration of preparation of IND-HTs/Gel for improving transdermal delivery.

Biotechnology Co., Ltd. (Hefei, China). Carbopol 940 was purchased from Lubrizol (Wickliffe, OH). All other reagents were analytical grade preparation.

### Animals

ICR mice (male, 18–22 g weight) were purchased from the Henan Experimental Animal Center, Zhengzhou, China. All of the animals were housed in temperature controlled (23–25 °C) rooms under a 12 h light cycle and had free access to food and tap water before the experiments. The experimental protocols were in accordance with the guidelines approved by Luoyang Normal University, and the study was approved by the Institutional Animal Ethics Committee.

### Synthesis of HA conjugated ODA

The amphiphilic HA-conjugated ODA (HA–ODA) was synthesized via an amide reaction (Song et al., 2017). Briefly, 100.0 mg of HA, 99.6 mg of EDC, and 59.8 mg of NHS were dissolved in 10 mL of deionized water and the mixture was stirred for 6 h at room temperature. 71.1 mg of ODA was dissolved in DMF, added dropwise into the previous reaction solution and stirred for 5 h at 60 °C. Then, the reaction was carried out at room temperature for another 24 h. The ultimate reaction product was dialyzed against excess amount of deionized water/ethanol (v/v, 1/3, 1/2, and 1/1) for 48 h followed by dialysis against water for 36 h and then collected by lyophilization. The HA–ODA was identified by $^{1}$H NMR using a 400 MHz apparatus (AVANCE500, Bruker, Karlsruhe, Germany) at 25 °C.

### Preparation and optimization of IND-HTs

Transfersomes were prepared by the thin film hydration method followed by membrane extrusion (Surini et al., 2020; Penoy et al., 2021). Briefly, SPC (1.5%, w/v), IND (0.5%, w/v), and HA–ODA (0%, 0.05%, 0.1%, 0.2%, 0.4%, and 0.6%, w/v) were dissolved in chloroform. The solution was then evaporated using a rotary vacuum evaporator (RE-52A, Yarong, Shanghai, China) at 35 °C to form a thin lipid film. The formed film was kept in a vacuum oven overnight for complete removal of solvent residuals. Subsequently, the thin film was hydrated in the deionized water with sodium deoxycholate (0.5%, w/v) at 35 °C and sonicated in an ice water bath for 5 min. The resulting transfersome suspension was extruded through the membrane with the pore size of 220 nm. The IND-loaded transfersomes not containing HA–ODA (IND-Ts) were prepared similar to the method above. The Cou6-loaded plain transfersomes (Cou6-Ts) and the Cou6-loaded HA-modified transfersomes (Cou6-HTs) were prepared by the same method, except that IND was replaced by Cou6 (0.027% of the SPC weight).

### Entrapment efficiency

The entrapment efficiency (EE%) of the tested formulations was determined by ultrafiltration with an ultrafiltration tube (molecular weight cut off: 30 kDa) and centrifugation for 10 min at 5000 rpm to completely filter out the dispersion medium. The filtrate was diluted with ethanol and quantified for the amount of IND using an ultraviolet-visible spectrophotometer (TU-1810PC, Purkinje, Beijing, China) at 320 nm. The content determination method was calibrated using standard solutions at different concentrations that ranged from 5 to 40 μg/mL of IND that was dissolved in ethanol ($R^2$=0.9997). The EE% was calculated using the following equation:

$$\text{EE}\ (\%)\ =\ (W_t - W_f)/W_t\ \times\ 100$$

where $W_t$ is the total amount of IND in the tested formulation and $W_f$ is the IND dispersed outside the nanovesicles.

### Size distribution and zeta potential

The particle size distribution and zeta potential of the formulations were determined via dynamic light scattering (DLS) using the instrument Zetasizer-3000 (Malvern, Worcestershire, UK) in triplicate. All samples were diluted 20-fold with distilled water for determination. The size distribution was expressed as the mean hydrodynamic diameter ($Z$ average) and polydispersity index (PDI).

### Morphology of IND-HTs

The morphology of IND-HTs was visualized by a scanning electron microscope (SEM) (Sigma 500, ZEISS, Oberkochen, Germany). Diluted suspension of IND-HTs was dropped onto a silicon substrate and dried overnight at room temperature. Subsequently, the silicon substrate was coated with gold of 10 nm thickness using a sputter coater under vacuum for allowing visualization, and observed by applying an acceleration voltage of 5.0 kV and 5.0 mm working distance.

### X-ray diffraction (XRD)

The XRD patterns of IND, physical mixture of IND and lipids, lyophilized blank HTs and IND-HTs were determined using an X-ray powder diffractometer (D8 ADVANCE, Bruker, Karlsruhe, Germany). Copper k-alpha radiation was used to substantiate probable drug carrier interactions. Additionally, the scanning rate was 5°/min, and the working voltage and current were 40 kV and 40 mA, respectively. Diffraction patterns were collected at 10–80° with $2\theta$.

### Fourier transform infrared spectroscopy (FTIR)

In order to characterize the status of IND in IND-HTs, FTIR analysis was performed with IND, physical mixture of IND and lipids, lyophilized blank HTs and IND-HTs, respectively. The spectra were obtained using a Nicolet 6700 FTIR Spectrophotometer (Thermo Fisher Scientific, Waltham, MA). The scans were obtained from 400 to 4000 $cm^{-1}$ at room temperature.

### Preparation of IND-HTs/gel

The IND-HTs/Gel was prepared using carbopol 940 as gel matrix (1%, w/w) (Pukale et al., 2020). Briefly, carbopol 940 (0.3 g) was hydrated with purified water (9.7 mL) overnight. Afterward triethanolamine (0.3 g) was added dropwise maintaining vigorous stirring until reaching the gel consistency and pH ~6.8. Freshly prepared IND-HTs 20 mL (equivalent to 0.1 g of IND) was added to the gel and stirred vigorously. Purified water was then added to make up the weight to 30 g and mixed well to obtain a visual homogeneity. IND-Ts/Gel, Cou6-Ts/Gel, and Cou6-HTs/Gel were prepared by the same method, except that IND-HTs were replaced by IND-Ts, Cou6-Ts, and Cou6-HTs, respectively. Blank gel was also prepared without IND-HTs dispersion. IND-HTs/Gel was lyophilized and the morphological evaluation of the lyophilized IND-HTs/Gel was determined using SEM as described above.

### In vitro *release studies*

*In vitro* release of hydrogel was determined by using vertical Franz diffusion cell (RYJ-6B, Shanghai, China) mounted with cellulose membrane (MWCO 3.5 kDa). The Franz diffusion cell, unlike the dialysis bags, is a commonly used apparatus to assess release of drugs from semisolid dosage forms of nanocarriers intended for application to the skin (Balzus et al., 2016; Zhang et al., 2018). The acceptor compartment was filled with 6.5 mL of phosphate buffer solution (PBS, pH 7.4) and the effective diffusion area was 2.8 $cm^2$. The receptor compartment was maintained at 37 ± 0.5 °C with a stirring speed of 300 rpm. The calculated amount of IND-HTs/Gel and IND-Ts/Gel was placed on the donor compartment. Samples (4.0 mL) were withdrawn at predetermined time intervals (2, 4, 8, 12, 24, and 48 h) from receptor compartment, and the same volume of fresh isothermal liquid (PBS, pH 7.4) was supplemented immediately. The samples were then analyzed using a high-performance liquid chromatography (HPLC) instrument (U-3000, Thermo, Waltham, MA) with a UV detector and a C18 column (Thermo, Waltham, MA, 5 μm, 200 × 4.6 mm). The composition of the mobile phase was 0.1% phosphoric acid:methanol (35:65, v/v) with a flow of 1 mL/min, and the column oven temperature was set at 35 °C. Samples were inspected at a detection wavelength of 228 nm and injection volume was 20 μL.

### Preparation of porcine ear skin

Porcine ears were freshly procured from recently slaughter animals (from a slaughterhouse authorized by the government sector for human consumption) and were cleaned with purified water. The hair on the dorsal side was removed using an electric shaver. The skin samples were obtained by separating the subcutaneous fat from the auricle's dorsal side, using a surgical scalpel; only regions without wounds, bruises, or warts were used (Mishra et al., 2016; de Oliveira et al., 2021). The biological tissues were stored in the refrigerator freezer and used for up to 30 days. Before the experiments, the skin samples were thawed at room temperature.

### In vitro *skin permeation studies*

The transdermal capability of the IND-HTs/Gel was investigated using the Franz diffusion cell system (Niu et al., 2020). The skin samples were mounted between the receptor and donor compartments of a diffusion cell with SC facing the donor compartment. The effective diffusion area of the diffused cells was 2.8 $cm^2$ and the volume of receptor compartment was 6.5 mL. The receptor compartments were filled with PBS (pH 7.4) maintained at 37 ± 0.5 °C with a stirring speed of 300 rpm. Subsequently, 0.5 g of the IND-HTs/Gel, IND-Ts/Gel, and free indomethacin hydrogel (IND/Gel) (equivalent to 1.67 mg of IND) were added to the donor compartment. Samples (2.0 mL) were withdrawn at predetermined time intervals (4, 6, 8, 10, 12, 24, 36, and 48 h) from receptor compartment and immediately replaced with fresh PBS. The samples were then analyzed using HPLC as described above.

After sampling, the skins were removed from the diffusion instrument and rinsed with deionized water to remove residual tested formulations. Then, the skins were cut into pieces with scissor and homogenized in 2 mL of methanol. The extract was centrifuged at 12,000 rpm for 10 min, and the supernatant was obtained. Indomethacin in the supernatant was analyzed by HPLC as described above.

The cumulative penetration amount per unit area at different sampling times ($Q_n$, μg/$cm^2$) was calculated as follows:

$$Q_n = \frac{VC_n + V_0 \sum_{i=0}^{n-1} C_i}{A}$$

where $C_n$ is the drug concentration in the receiving medium at different sampling times (μg/mL), $C_i$ is the drug concentration in the receiving medium at the *i*th ($n$ – 1) sampling time (μg/mL), $V$ is the volume of the receptor solution (mL), $V_0$ is the volume of the sample withdrawn (mL), and $A$ is the effective permeation area of the diffusion cell ($cm^2$). Measurements were performed in triplicate. The $Q_n$ values were plotted against time, and then the steady-state flux ($J_{ss}$) was calculated from the slope of the linear portion of the plot (Li et al., 2020; Zhang et al., 2020). To compare the permeation enhancement capacities of different formulations, the enhancement ratio (ER) was determined as follows: ER = ($J_{ss}$ of IND transfersome hydrogel)/($J_{ss}$ of free IND hydrogel).

### Ex vivo *bioimaging*

Coumarin 6 (Cou6), a common fluorescent dye, was used to examine the *ex vivo* distribution of HTs in the porcine ear skin (Pukale et al., 2020). The porcine ear skin was mounted between the donor and receptor compartment that was held tightly by clamps in Franz's diffusion cells with the contact surface area of 2.8 $cm^2$. The receptor compartment was filled with PBS (6.5 mL; pH 7.4). In the donor compartment, Cou6-Ts/Gel and Cou6-HTs/Gel (equivalent to 1.33 μg of Cou6)

were taken, followed by incubation for 4 h and 8 h at 37 ± 0.5 °C at stirring speed of 300 rpm. At each time point, skin samples were collected from the Franz diffusion cells and washed with PBS (pH 7.4). The skin region that received the hydrogel was excised, frozen at −80 °C, and then vertically sliced with a freezing slicer (Leica CM 1950, Wetzlar, Germany). The tissue sections were nucleus counterstained with DAPI and visualized by CaseViewer 2.3 (3DHISTECH Ltd., Budapest, Hungary).

### *Hematoxylin–eosin staining*

Permeation studies were performed under the same conditions as described in the *in vitro* skin permeation studies. Saline, IND/Gel, IND-Ts/Gel, and IND-HTs/Gel were added to the donor compartment of the Franz diffusion cells. After application for 12 h, skin samples were collected and then fixed in 4% paraformaldehyde at 4 °C, dehydrated in a graded series of ethanol, made transparent with xylene, embedded in paraffin, sliced, stained with hematoxylin–eosin (HE), sealed with neutral gum, and observed for histology analysis using CaseViewer 2.3 (3DHISTECH Ltd., Budapest, Hungary) (Yang et al., 2019).

### In vivo *analgesic activity evaluation*

*In vivo* analgesic activity was determined by modified hot plate test (Aziz et al., 2019). The mice were individually placed on top of hot plate at constant temperature of 55 °C (Wang et al., 2016). The reaction time (s) between the mice place onto the apparatus and the nociceptive response occurrence (licking or shaking the hind paws) was recorded. The tested mice were divided into four groups, which were treated on the planta with 0.4 g of blank gel, IND/Gel, IND-Ts/Gel, and IND-HTs/Gel for 30 min. The mice were tested before treatments and 30, 60, and 90 min after treatments. Maximum reaction time was fixed at 60 s to prevent any injury to the tissues of mice paws. If the reading exceeds 60 s, it would be considered as maximum analgesia.

### *Acute dermal irritation test*

The dermal irritation/corrosion properties of the gel formulations were assessed in mice according to the previous study (Niu et al., 2020). Mice were anesthetized by intraperitoneal injection of 2% chloral hydrate (0.15 mL/10 g) and their dorsum (approximately 3 cm × 3 cm) were shaved 24 h before the test without causing tissue damage. Then, the dorsum of the mice was washed with purified water. After mice were dried, 0.5 g of the IND-HTs/Gel and normal saline (control) were applied to the shaved patches of skin. Each group was consisted of six mice. After 4 h of treatment, the residual formulations were removed with warm water. At 1, 4, 24, 48, and 72 h after removing the residual formulations, all mice were visually examined. Assessment of skin irritation was made through visual analysis of the edema and/or erythema and classified according to Table 1. Scores for erythema and edema were summed and divided by the number of the observations for the treated sites. The primary skin irritation degree was calculated as the arithmetical mean of the six mice. The irritation degree was categorized as nonirritating (score 0–1.0); slight irritation (score 1.1–2.0); severe irritation (score 2.1–3.0); corrosive (score >3.1).

### *Statistical analysis*

Data were expressed as mean ± standard deviations (SDs) from at least three independent experiments. The statistical differences between two groups were evaluated using Student's *t*-test and considered significant for $p < .05$ ($^{*}p < .05$; $^{**}p < .01$; $^{***}p < .001$).

## Results and discussion

### *Optimization and characterization of IND-HTs formulation*

Low molecular weight HA (<10 kDa) was used in the preparation of IND-HTs, because it showed a significantly higher skin penetration rate than larger weight HA. If the molecular weight of HA was too large, the drug would be trapped in an entangled network with limited mobility, which eventually limited the permeability of the formulation. HA was a water-soluble polymer, which could be coated on the surface of transfersomes. However, this modification was instable and HA molecules would detach when the concentration of transfersomes changed greatly (Zhang et al., 2019). To enable the successful modification of HA on the surface of the transfersomes, HA and ODA were covalently bonded (Figure 2(A)). In the preparation of IND-HTs, HA–ODA could be inserted into the phospholipid bilayer, while the HA molecules were exposed on the surface of the transfersomes. The HA–ODA was synthesized by a coupling reaction between the carboxyl groups of HA and the amino groups of ODA. The chemical structures of HA, ODA, and HA–ODA were identified by $^{1}$H NMR analysis (Figure 2(B)). The characteristic peak of HA–ODA at 1.91 ppm was attributed to the N-acetyl (–$NHCOCH_3$). The peaks ranging from 3.01 to 4.03 ppm were attributed to the protons in the sugar ring of HA. The peak at 0.97 ppm corresponded to the methyl (–$CH_3$) of ODA. The

Table 1. Classification for skin reaction.

| Erythema | Score | Edema | Score |
|---|---|---|---|
| No erythema | 0 | No edema | 0 |
| Very slight erythema | 1 | Very slight edema | 1 |
| Well defined erythema | 2 | Well defined edema (edges of the area well defined by define raising) | 2 |
| Moderate to severe erythema | 3 | Moderate edema (raising approximately 1 mm) | 3 |
| Severe erythema (beet redness) to eschar formation | 4 | Severe edema (raised more than 1 mm and extended beyond the area of exposure) | 4 |

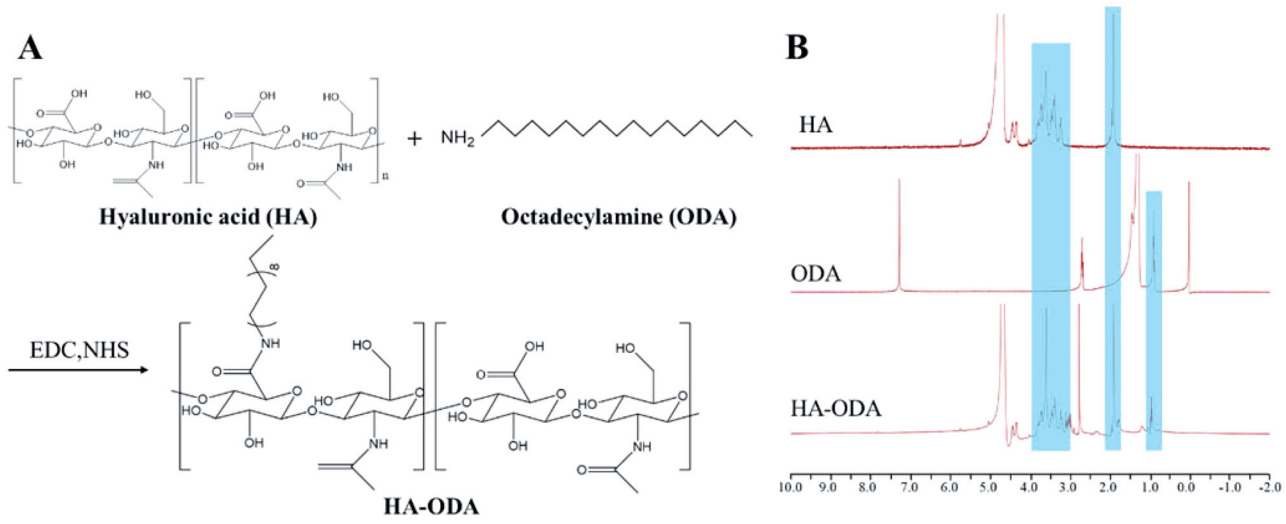


**Figure 2.** (A) Synthetic scheme for HA–ODA; (B) $^{1}$H NMR spectra of HA, ODA, and HA–ODA.

**Table 2.** Optimization of the IND-HTs formulation.

| HA (%, w/v) | Average diameter (nm) | PDI | EE% | Zeta potential (mV) |
|---|---|---|---|---|
| 0 | 143.6 ± 48.52 | 0.11 ± 0.02 | 84.31 ± 3.14 | −34.4 ± 0.68 |
| 0.05 | 163.0 ± 56.37 | 0.12 ± 0.02 | 71.24 ± 1.26 | −42.1 ± 1.37 |
| 0.1 | 179.3 ± 72.57 | 0.16 ± 0.01 | 72.39 ± 1.72 | −41.0 ± 0.53 |
| 0.2 | 180.0 ± 45.95 | 0.07 ± 0.03 | 76.29 ± 3.57 | −36.4 ± 0.51 |
| 0.4 | 221.8 ± 93.34 | 0.17 ± 0.02 | 87.88 ± 2.03 | −34.4 ± 1.67 |
| 0.6 | 201.1 ± 76.70 | 0.15 ± 0.01 | 83.47 ± 1.82* | −31.2 ± 0.36 |
| 0.8 | 235.7 ± 97.95 | 0.17 ± 0.02 | 81.61 ± 4.51 | −31.0 ± 1.21 |

*$p < .05$ compared with the EE% when the concentration of HA–ODA was 0.4%.

results verified that the HA–ODA conjugate was successfully constructed.

The IND-HTs were consisted by phospholipid, sodium deoxycholate, and HA–ODA. The optimal amount of HA–ODA used in the formulation was determined by the size and EE% of the IND-HTs, and the results are shown in Table 2. The EE% was increased as the concentration of HA–ODA ranging from 0.05% to 0.4%. When the concentration of HA–ODA exceeded 0.4%, the EE% was significantly decreased ($p < .05$). This might be because the insertion of excessive HA–ODA into the phospholipid bilayer causing drug leakage and a decrease in drug EE% (Zhang et al., 2019). The EE% of IND-HTs reached the highest value (87.88 ± 2.03%) when the concentration of HA–ODA was 0.4%. The sizes of all the transfersome formulations were smaller than 300 nm, which were reported to deliver the contents into deep layers of the skin (Zhang et al., 2018). Considering the EE% and particle size, the final concentration of HA–ODA in the preparation was selected as 0.4%. In addition, PDI values of the formulated IND-HTs were smaller than 0.2, indicating relative narrow size distribution. The zeta potential was less than −30 mV, providing an electrostatic repulsion force between particles to avoid aggregation or flocculation, indicating good physical stability.

The SEM image confirmed the well-defined spherical shapes and homogeneous distribution of IND-HTs (Figure 3(A)). In addition, after freeze-drying, the IND-HTs/Gel showed a typical 3D porous morphology and the transfersomes disperse in the pore structure with no visible aggregation (indicated by the yellow arrow; Figure 3(B)).

### X-ray diffraction

To elucidate the crystalline properties of the drug in the lipid carrier, the XRD patterns of pure IND, physical mixture, blank HTs, and IND-HTs were studied (Figure 4). XRD pattern of IND showed the sharp and intense peak, indicating its high crystallinity at $2\theta$ values of 12.7°, 18.3°, 19.6°, 28.1°, and 39.9° (Lenz et al., 2015). The diffraction pattern of blank HTs showed two weak peaks at $2\theta$ of 14.9° and 20.9°. XRD diffractogram of physical mixture showed the typical peaks of IND which confirmed the crystalline form of IND. However, the characteristic peaks of IND were disappeared for the IND-HTs, indicating that IND was converted from the crystalline structure to an amorphous state encapsulated within the transfersome matrix. A similar phenomenon has been described in the previous literature (Li et al., 2018; Niu et al., 2020). Amorphous IND had greater free energy, which was contributed to enhance solubility and release of drug, and further improved skin bioavailability.

### FTIR characterization

FTIR analysis was also employed for the characterization of IND-HTs. Usually, the interaction of drug with lipid carriers could lead to identifiable changes in FTIR spectra. The FTIR spectra of IND, physical mixture, blank HTs, and IND-HTs are shown in Figure 5. For IND, the typical bands at 1720 $cm^{-1}$ and 1690 $cm^{-1}$ were due to the carbonyl stretching of carboxylic acid and amide, respectively (Badri et al., 2017). For blank HTs, the bands at 2926 $cm^{-1}$ (the $CH_2$ stretching vibration) and 1738 $cm^{-1}$ (symmetrical C=O stretching vibration) were regarded as characteristic for phospholipids (Li et al., 2018). The spectrum of IND-HTs was basically similar to that of blank HTs, while the characteristic peaks of IND at 1720 $cm^{-1}$ and 1690 $cm^{-1}$ were disappeared. This change

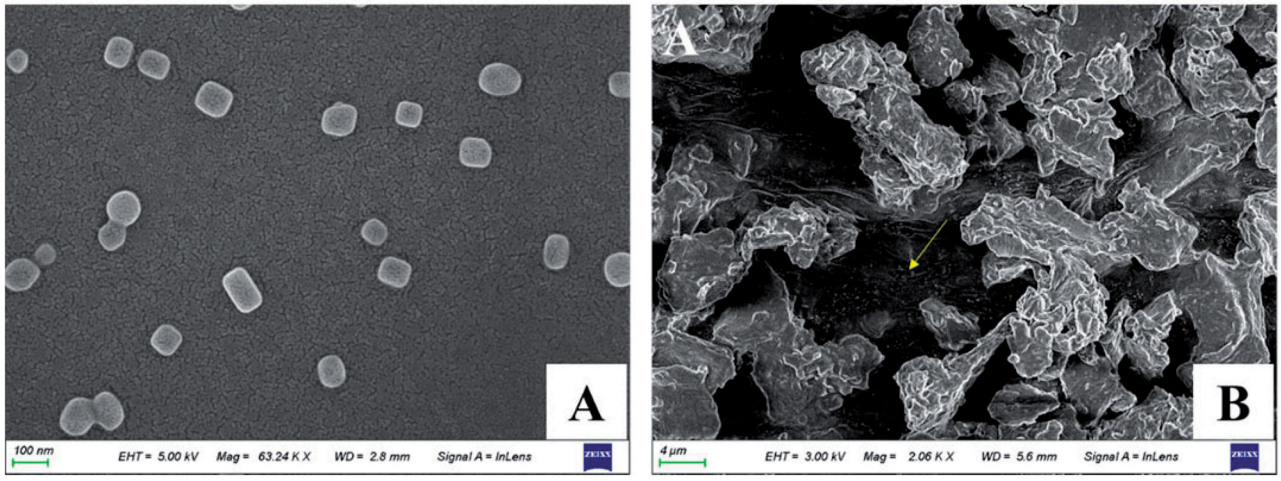


**Figure 3.** SEM images of IND-HTs (A) and lyophilized IND-HTs/Gel (B). The yellow arrow indicated the transfersomes dispersed in the 3D pore structure of the hydrogel.

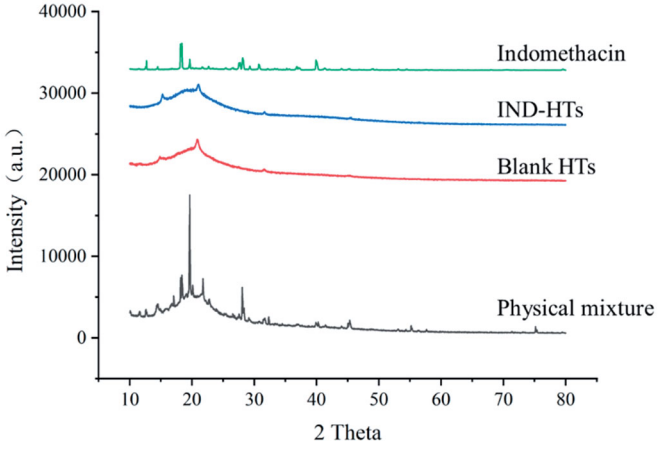


**Figure 4.** XRD patterns of indomethacin, IND-HTs, blank HTs, and physical mixture.

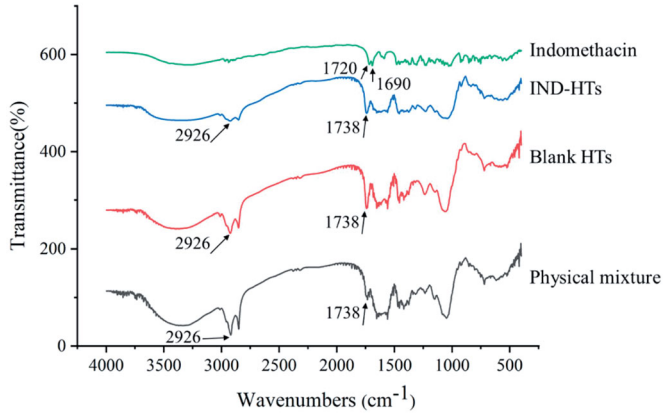


**Figure 5.** FTIR spectra of indomethacin, IND-HTs, blank HTs, and physical mixture.

might be attributed to hydrogen bonding between phospholipids and carbonyl groups of IND (Saboo et al., 2020).

## In vitro *drug release study*

To increase the skin retention property of the IND-HTs, carbopol hydrogel was employed as a reservoir to entrap the IND-HTs. The vertical Franz diffusion cell, unlike the dialysis bags, was a commonly used apparatus to assess release of semisolid dosage forms of nanocarriers intended for application to the skin (Kilfoyle et al., 2012; Balzus et al., 2016). The *in vitro* release behaviors of IND from IND-Ts/Gel and IND-HTs/Gel are shown in Figure 6(A). In the first 2 h, the drug release from IND-Ts/Gel and IND-HTs/Gel was 12.9% and 9.7%, respectively. At 48 h, the cumulative release of IND-Ts/Gel was 68.8%, while IND-HTs/Gel showed a lower release of 48.5% ($p < .01$). HA modification on the surface of the transfersomes resulted in a significant lower release rate of IND-HTs/Gel. This could help the drug diffused from the transfersomes into the skin layers, rather than the drug released before the vesicles permeated into the skin.

## In vitro *skin penetration and retention*

Transdermal drug permeation of IND-HTs/Gel across porcine ear skin was quantitatively studied using the Franz diffusion cell. IND/Gel was used as the control group. As shown in Figure 6(B), over 48 h exposure, the cumulative drug permeation ($Q_t$, μg/cm$^2$) through the skin increased with time for all formulations. After 48 h of penetration, the $Q$ values of IND/Gel, IND-Ts/Gel, and IND-HTs/Gel were 56.54 ± 6.43 μg/cm$^2$, 99.09 ± 31.58 μg/cm$^2$, and 171.73 ± 30.29 μg/cm$^2$, respectively. The cumulative drug permeation of IND-HTs/Gel was significantly higher than that of IND/Gel ($p < .01$). IND-Ts/Gel and IND-HTs/Gel showed a favorable percutaneous permeability. This might be attributed to deformable structure to efficiently penetrate through the small channels in the skin. In addition, the surfactants incorporated in the transfersomes increased SC lipid fluidity and decreased the density of lipid layers.

It also could be seen that IND-HTs/Gel penetration more effectively than IND-Ts/Gel ($p < .05$), which indicated the advantage of HA in penetration. At 48 h after transdermal administration, the $Q$ value of IND-HTs was 171.73 ± 30.29 μg/cm$^2$, which was about 1.73 times enhancement than that of

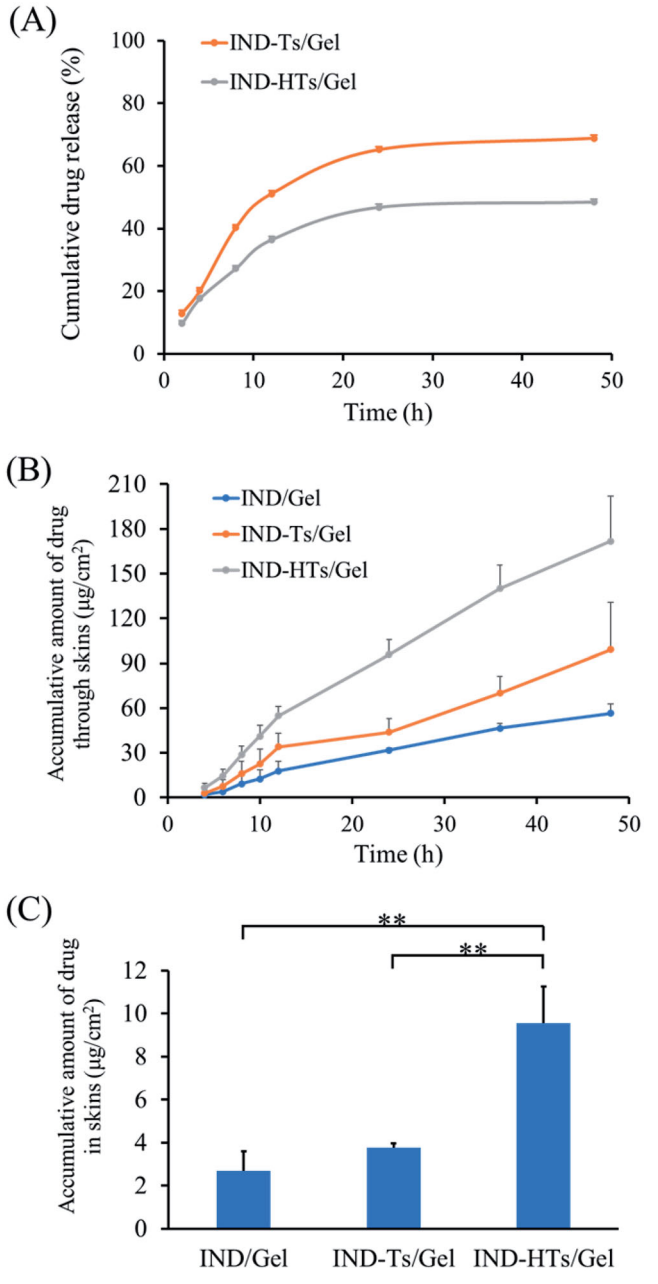


**Figure 6.** (A) *In vitro* profiles of indomethacin release from IND-Ts/Gel and IND-HTs/Gel. (B) *In vitro* skin permeation profiles of indomethacin from IND/Gel, IND-Ts/Gel, and IND-HTs/Gel. (C) Indomethacin retention in porcine ear skin after exposure to IND/Gel, IND-Ts/Gel, and IND-HTs/Gel for 48 h. Results were presented as mean ± SD ($n = 3$; $^{**}p < .01$).

IND-Ts/Gel. HA was a hygroscopic molecular that could hydrate both the SC and the dermis. The extensive hydration would lead to swollen corneocytes, causing the microstructural changes in lipid self-assembly, and eventually facilitating the permeation through the hydrated skin. Table 3 shows the steady state flux ($J_{ss}$) that is calculated from the linear part of the cumulative permeation per area versus time plot. IND-HTs/Gel presented the highest $J_{ss}$ value followed by IND-Ts/Gel and IND/Gel in sequence, which was consistent with the above results.

The amount of IND deposited in the skin is shown in Figure 6(C). IND-HTs/Gel showed a significantly higher ($p < .01$) drug deposition in skin than that of IND-Ts/Gel.

**Table 3.** *In vitro* permeation parameters of IND/Gel, IND-Ts/Gel, and IND-HTs/Gel through excised porcine ear skin ($n = 3$).

| Formulations | $J_{ss}$ (μg/cm$^2$·h) | Enhancement ratio (ER) |
|---|---|---|
| IND/Gel | 1.11 ± 0.28 | 1.00 |
| IND-Ts/Gel | 1.98 ± 0.60 | 1.78 |
| IND-HTs/Gel | 3.67 ± 0.59$^{**,\#}$ | 3.31 |

Data were expressed as mean ± SD ($n = 3$).
$^{**}p < .01$ compared with the IND/Gel.
$\#p < .05$ compared with IND-Ts/Gel.

IND-HTs/Gel improved the drug deposition 2.54 times enhancement compared with IND-Ts/Gel. This was in agreement with previous literature, which might be due to that: (i) low molecular weight HA had a strong affinity to keratin in the SC (Cilurzo et al., 2014), and exhibited epidermal retention effect and (ii) the viscoelastic property of HA contributed to retain in epidermis for a longer time. Drug molecule would be trapped in an entangled network of HA chains in viable epidermis (Zhu et al., 2020). Indomethacin was commonly taken orally, but it was also available in topical preparations to be applied to or rubbed onto the skin, with the aim of relieving inflammatory pain locally. Therefore, IND deposited in the skin could increase local concentrations, acting as a drug reservoir and avoiding side-effects (Puglia et al., 2004; Yassin et al., 2015).

## *Fluorescence microscopy imaging*

An *ex vivo* skin permeation study was performed to confirm the enhanced transdermal effect of HA using Franz's diffusion cells and confocal laser scanning microscopy (CLSM) images. Cou6 was used as a lipophilic fluorescent dye to easily observe the skin distribution. The CLSM images of vertical section of porcine ear skin treated with Cou6-Ts/Gel and Cou6-HTs/Gel are shown in Figure 7. After 4 h of permeation, very weak fluorescence was observed in the skin treated with Cou6-Ts/Gel. In contrast, Cou6-HTs/Gel group was observed with enhanced fluorescence in epidermis layers. After 8 h of permeation, Cou6-HTs/Gel group localized in the deep skin layers, and showed stronger fluorescence compared to Cou6-Ts/Gel group. The results demonstrated the superiority of HTs/Gel for percutaneous penetration and drug retention.

## *HE stained*

To study the transdermal mechanism of IND-HTs, skin tissues were HE stained and microscopically observed. The histological photomicrographs of skin treated with saline, IND/Gel, IND-Ts/Gel, and IND-HTs/Gel are shown in Figure 8. In the normal saline group, the skin structure was complete, the layers of epidermis were closely arranged and the stratification was clear. The keratin cells were closely connected, and fewer keratin fragments could be observed. After treatment with IND/Gel and IND-Ts/Gel, the keratin fragment increased and the skin layers were still clear. However, the microstructure of the skin treated with IND-HTs/Gel was obviously

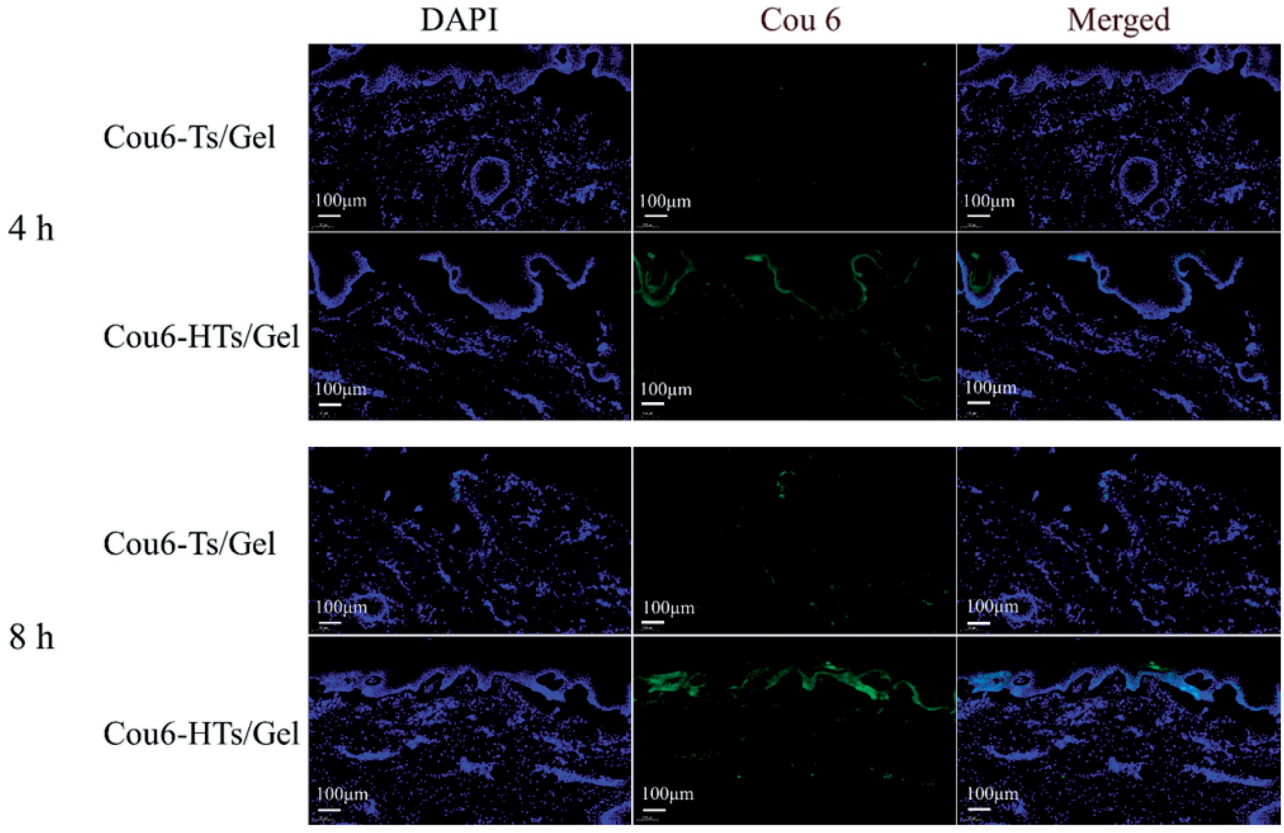


**Figure 7.** CLSM images of longitudinal section of the skins incubated with Cou6-Ts/Gel and Cou6-HTs/Gel at 4 h and 8 h (scale bar: 100 μm).

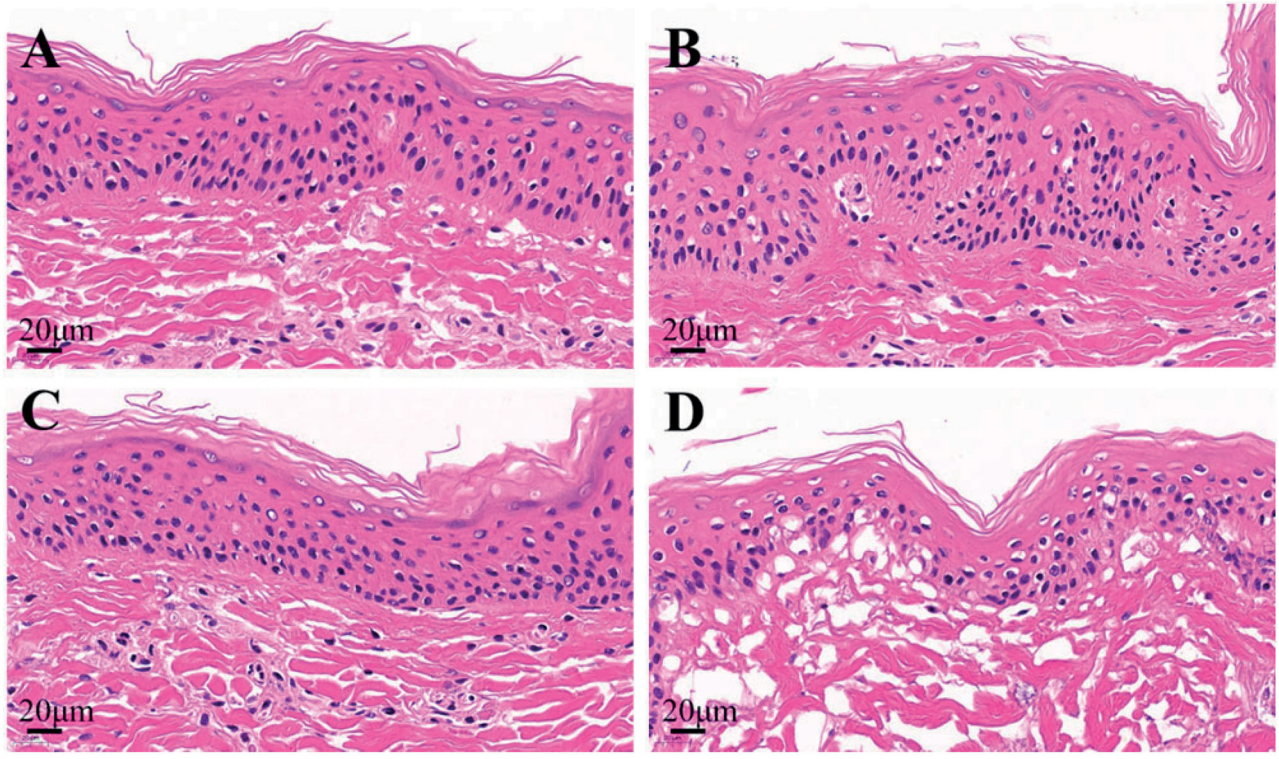


**Figure 8.** Histological photomicrographs of skins stained with HE after incubated with saline (A), IND/Gel (B), IND-Ts/Gel (C), and IND-HTs/Gel (D) (scale bar: 20 μm).

changed. The SC was loose and thin, the keratin fragment increased, the intercellular space in the spinous layer increased, and the basal layer cells were loosely arranged. The results indicated that skins treated with IND/Gel and IND-Ts/Gel remained complete microstructure, whereas the skin barrier of IND-HTs/Gel group was disrupted. It could be

Table 4. The pain reaction time of mice after application of blank gel, IND/Gel, IND-Ts/Gel, and IND-HTs/Gel.

| | Reaction time (s) | | | |
|---|---|---|---|---|
| | Blank gel | IND/Gel | IND-Ts/Gel | IND-HTs/Gel |
| Before treatment | 16.2 ± 3.47 | 15.5 ± 3.06 | 16.7 ± 2.97 | 14.1 ± 2.89 |
| After treatment 30 min | 16.6 ± 4.45 | 16.4 ± 6.32 | 18.3 ± 6.72 | 15.9 ± 6.81 |
| After treatment 60 min | 16.8 ± 5.74 | 17.0 ± 5.07 | 19.4 ± 7.21 | 18.1 ± 6.47 |
| After treatment 90 min | 16.9 ± 5.21 | 17.7 ± 5.84 | 21.3 ± 5.45 | 22.3 ± 3.62*,# |

Data were represented as mean ± SD ($n = 10$).
*$p < .05$ compared with blank gel.
#$p < .05$ compared with IND/Gel.

Table 5. Primary skin irritation scores for IND-HTs.

| | IND-HTs/Gel | | Control | |
|---|---|---|---|---|
| Time after application (h) | Edema | Erythema | Edema | Erythema |
| 1 | 0 | 0 | 0 | 0 |
| 4 | 0 | 0 | 0 | 0 |
| 24 | 0 | 0 | 0 | 0 |
| 48 | 0 | 0 | 0 | 0 |
| 72 | 0 | 0 | 0 | 0 |

inferred that HA improved the transdermal effect by changing the microstructure of skins. This might be because the skin hydration effect of HA. HA was a hygroscopic molecular and was able to hydrate both the SC and the dermis. The extensive hydration would lead to swollen corneocytes, separation of lipid bilayers, and eventually facilitating the permeation through the hydrated skin. The disruptions of skin structure were reversible. Once the hydration resource was removed, the skin barriers would be restored (Tan et al., 2010).

### *Assessment of analgesic activity*

*In vivo* analgesic activity was studied by hot plate method in mice. Table 4 shows the results of mean reaction time toward thermal stimulus pain after treated on planta with blank gel, IND/Gel, IND-Ts/Gel, and IND-HTs/Gel. As shown in the table, IND-HTs/Gel group showed a significant prolonged time of mice responses toward the thermal pain, compared to blank gel which reported to be no significant increase of reaction time within overall 90 min of treatment. What is more, the potential of IND/Gel and IND-Ts/Gel to prolong the reaction time was both lower than IND-HTs/Gel at all tested time points. The results suggested the successful inhibitory effects of IND-HTs/Gel on peripheral analgesic activities.

### *Acute skin irritation test*

The skin irritation test was carried out to evaluate primary skin irritation potential of the developed hydrogel formulations. The primary skin irritation scores are shown in Table 5. During the experiment, no erythema or edema was observed in mice exposed to IND-HTs/Gel. Therefore, the developed formulation was considered as nonirritating and safe for topical use.

## Conclusions

In this study, a hydrogel containing HA-modified transfersomes was successfully prepared as a novel drug carrier for IND. The IND-HTs presented favorable transdermal efficiency by the aid of HA modification on the surface of the vesicles. HA disturbed the skin barriers and then the deformable IND-HTs could efficiently squeeze through the increased intercellular space. *In vitro* skin permeation study illustrated that IND-HTs/Gel promoted drug permeation through the skin and the penetration enhancement potential was further confirmed by CLSM in comparison to the IND-Ts/Gel. *In vivo* study indicated that IND-HTs/Gel showed superior antinociceptive activity and high safety for topical use. Accordingly, this topical drug delivery system could be considered a promising noninvasive approach to enhance skin permeation and transdermal delivery.

## Disclosure statement

No potential conflict of interest was reported by the author(s).

## Funding

We appreciate the financial supports from Applied Science and Technology Research Fund of Luoyang Normal University (No. 2018-YYJJ-004), the Key Scientific Research Project of Higher Education of Henan Province (No. 20B180006), and National Level Project Cultivation Fund of Luoyang Normal University (No. 2019-PYJJ-012; No. 2018-PYJJ-007).

## References

Abd El-Alim SH, Kassem AA, Basha M, et al. (2019). Comparative study of liposomes, ethosomes and transfersomes as carriers for enhancing the transdermal delivery of diflunisal: in vitro and in vivo evaluation. Int J Pharm 563:293–303.

Alkilani AZ, McCrudden MT, Donnelly RF. (2015). Transdermal drug delivery: innovative pharmaceutical developments based on disruption of the barrier properties of the stratum corneum. Pharmaceutics 7: 438–70.

Andrews SN, Jeong E, Prausnitz MR. (2013). Transdermal delivery of molecules is limited by full epidermis, not just stratum corneum. Pharm Res 30:1099–109.

Ascenso A, Raposo S, Batista C, et al. (2015). Development, characterization, and skin delivery studies of related ultradeformable vesicles: transfersomes, ethosomes, and transethosomes. Int J Nanomedicine 10:5837–51.

Aziz ZAA, Nasir HM, Ahmad A, et al. (2019). Enrichment of Eucalyptus oil nanoemulsion by micellar nanotechnology: transdermal analgesic activity using hot plate test in rats' assay. Sci Rep 9:13678.

Badri W, Miladi K, Robin S, et al. (2017). Polycaprolactone based nanoparticles loaded with indomethacin for anti-inflammatory therapy: from preparation to ex vivo study. Pharm Res 34:1773–83.

Balzus B, Colombo M, Sahle FF, et al. (2016). Comparison of different in vitro release methods used to investigate nanocarriers intended for dermal application. Int J Pharm 513:247–54.

Batool S, Zahid F, Ud-Din F, et al. (2021). Macrophage targeting with the novel carbopol-based miltefosine-loaded transfersomal gel for the treatment of cutaneous leishmaniasis: in vitro and in vivo analyses. Drug Dev Ind Pharm 47:440–53.

Cilurzo F, Vistoli G, Gennari CG, et al. (2014). The role of the conformational profile of polysaccharides on skin penetration: the case of hyaluronan and its sulfates. Chem Biodivers 11:551–61.

de Oliveira EL, Ferreira SBS, de Castro-Hoshino LV, et al. (2021). Thermoresponsive hydrogel-loading aluminum chloride phthalocyanine as a drug release platform for topical administration in photodynamic therapy. Langmuir 37:3202–13.

El-Leithy ES, Ibrahim HK, Sorour RM. (2015). In vitro and in vivo evaluation of indomethacin nanoemulsion as a transdermal delivery system. Drug Deliv 22:1010–7.

Guermech I, Lassoued MA, Abdelhamid A, et al. (2019). Development and assessment of lipidic nanoemulsions containing sodium hyaluronate and indomethacin. AAPS PharmSciTech 20:330.

Khan AU, Jamshaid H, Ud Din F, et al. (2022). Designing, optimization and characterization of trifluralin transfersomal gel to passively target cutaneous leishmaniasis. J Pharm Sci;

Kilfoyle BE, Sheihet L, Zhang Z, et al. (2012). Development of paclitaxel-TyroSpheres for topical skin treatment. J Control Release 163:18–24.

Laurent TC, Fraser JR. (1992). Hyaluronan. FASEB J 6:2397–404.

Lenz E, Jensen KT, Blaabjerg LI, et al. (2015). Solid-state properties and dissolution behaviour of tablets containing co-amorphous indomethacin–arginine. Eur J Pharm Biopharm 96:44–52.

Li ZL, Peng SF, Chen X, et al. (2018). Pluronics modified liposomes for curcumin encapsulation: sustained release, stability and bioaccessibility. Food Res Int 108:246–53.

Li H, Peng Q, Guo Y, et al. (2020). Preparation and in vitro and in vivo study of asiaticoside-loaded nanoemulsions and nanoemulsions-based gels for transdermal delivery. Int J Nanomedicine 15:3123–36.

Maestrelli F, Gonzalez-Rodriguez ML, Rabasco AM, et al. (2010). New "drug-in cyclodextrin-in deformable liposomes" formulations to improve the therapeutic efficacy of local anaesthetics. Int J Pharm 395:222–31.

Mishra R, Prabhavalkar KS, Bhatt LK. (2016). Preparation, optimization, and evaluation of zaltoprofen-loaded microemulsion and microemulsion-based gel for transdermal delivery. J Liposome Res 26:297–306.

Mura P, Maestrelli F, Gonzalez-Rodriguez ML, et al. (2007). Development, characterization and in vivo evaluation of benzocaine-loaded liposomes. Eur J Pharm Biopharm 67:86–95.

Niu J, Yuan M, Chen C, et al. (2020). Berberine-loaded thiolated Pluronic F127 polymeric micelles for improving skin permeation and retention. Int J Nanomedicine 15:9987–10005.

Penoy N, Grignard B, Evrard B, et al. (2021). A supercritical fluid technology for liposome production and comparison with the film hydration method. Int J Pharm 592:120093.

Puglia C, Trombetta D, Venuti V, et al. (2004). Evaluation of in-vivo topical anti-inflammatory activity of indometacin from liposomal vesicles. J Pharm Pharmacol 56:1225–32.

Pukale SS, Sharma S, Dalela M, et al. (2020). Multi-component clobetasol-loaded monolithic lipid-polymer hybrid nanoparticles ameliorate imiquimod-induced psoriasis-like skin inflammation in Swiss albino mice. Acta Biomater 115:393–409.

Qindeel M, Ullah MH, Fakhar UD, et al. (2020). Recent trends, challenges and future outlook of transdermal drug delivery systems for rheumatoid arthritis therapy. J Control Release 327:595–615.

Rabia S, Khaleeq N, Batool S, et al. (2020). Rifampicin-loaded nanotransferosomal gel for treatment of cutaneous leishmaniasis: passive targeting via topical route. Nanomedicine 15:183–203.

Saboo S, Kestur US, Flaherty DP, et al. (2020). Congruent release of drug and polymer from amorphous solid dispersions: insights into the role of drug–polymer hydrogen bonding, surface crystallization, and glass transition. Mol Pharm 17:1261–75.

Sala M, Diab R, Elaissari A, et al. (2018). Lipid nanocarriers as skin drug delivery systems: properties, mechanisms of skin interactions and medical applications. Int J Pharm 535:1–17.

Salim MW, Shabbir K, ud-Din F, et al. (2020). Preparation, in-vitro and in-vivo evaluation of rifampicin and vancomycin co-loaded transfersomal gel for the treatment of cutaneous leishmaniasis. J Drug Deliv Sci Technol 60:101996.

Singh D, Pradhan M, Nag M, et al. (2015). Vesicular system: versatile carrier for transdermal delivery of bioactives. Artif Cells Nanomed Biotechnol 43:282–90.

Son SU, Lim JW, Kang T, et al. (2017). Hyaluronan-based nanohydrogels as effective carriers for transdermal delivery of lipophilic agents: towards transdermal drug administration in neurological disorders. Nanomaterials 7:427.

Song L, Pan Z, Zhang H, et al. (2017). Dually folate/CD44 receptor-targeted self-assembled hyaluronic acid nanoparticles for dual-drug delivery and combination cancer therapy. J Mater Chem B 5:6835–46.

Surini S, Leonyza A, Suh CW. (2020). Formulation and in vitro penetration study of recombinant human epidermal growth factor-loaded transfersomal emulgel. Adv Pharm Bull 10:586–94.

Tan G, Xu P, Lawson LB, et al. (2010). Hydration effects on skin microstructure as probed by high-resolution cryo-scanning electron microscopy and mechanistic implications to enhanced transcutaneous delivery of biomacromolecules. J Pharm Sci 99:730–40.

Touitou E, Dayan N, Bergelson L, et al. (2000). Ethosomes – novel vesicular carriers for enhanced delivery: characterization and skin penetration properties. J Control Release 65:403–18.

Wang Y, Wang S, Shi P. (2016). Transcriptional transactivator peptide modified lidocaine-loaded nanoparticulate drug delivery system for topical anesthetic therapy. Drug Deliv 23:3193–9.

Yang JA, Kim ES, Kwon JH, et al. (2012). Transdermal delivery of hyaluronic acid – human growth hormone conjugate. Biomaterials 33: 5947–54.

Yang W, Xu H, Lan Y, et al. (2019). Preparation and characterisation of a novel silk fibroin/hyaluronic acid/sodium alginate scaffold for skin repair. Int J Biol Macromol 130:58–67.

Yassin NZ, El-Shenawy SM, Abdel-Rahman RF, et al. (2015). Effect of a topical copper indomethacin gel on inflammatory parameters in a rat model of osteoarthritis. Drug Des Devel Ther 9:1491–8.

Zhang Y, Ng W, Hu J, et al. (2018). Formulation and in vitro stability evaluation of ethosomal carbomer hydrogel for transdermal vaccine delivery. Colloids Surf B Biointerfaces 163:184–91.

Zhang Y, Xia Q, Li Y, et al. (2019). CD44 assists the topical anti-psoriatic efficacy of curcumin-loaded hyaluronan-modified ethosomes: a new strategy for clustering drug in inflammatory skin. Theranostics 9: 48–64.

Zhang ZJ, Osmałek T, Michniak-Kohn B. (2020). Deformable liposomal hydrogel for dermal and transdermal delivery of meloxicam. Int J Nanomedicine 15:9319–35.

Zhu J, Tang X, Jia Y, et al. (2020). Applications and delivery mechanisms of hyaluronic acid used for topical/transdermal delivery – a review. Int J Pharm 578:119127.